

Efficiently Processing Large Relational Joins on GPUs

Bowen Wu
Systems Group
ETH Zurich, Switzerland
bowen.wu@inf.ethz.ch

Dimitrios Koutsoukos
Systems Group
ETH Zurich, Switzerland
dkoutsou@inf.ethz.ch

Gustavo Alonso
Systems Group
ETH Zurich, Switzerland
alonso@inf.ethz.ch

ABSTRACT

With the growing interest in Machine Learning (ML), Graphic Processing Units (GPUs) have become key elements of any computing infrastructure. Their widespread deployment in data centers and the cloud raises the question of how to use them beyond ML use cases, with growing interest in employing them in a database context. In this paper, we explore and analyze the implementation of relational joins on GPUs from an end-to-end perspective, meaning that we take result materialization into account. We conduct a comprehensive performance study of state-of-the-art GPU-based join algorithms over diverse synthetic workloads and TPC-H/TPC-DS benchmarks. Without being restricted to the conventional setting where each input relation has only one key and one non-key with all attributes being 4-bytes long, we investigate the effect of various factors (e.g., input sizes, number of non-key columns, skewness, data types, match ratios, and number of joins) on the end-to-end throughput. Furthermore, we propose a technique called “Gather-from-Transformed-Relations” (GFTR) to reduce the long-ignored yet high materialization cost in GPU-based joins. The experimental evaluation shows significant performance improvements from GFTR, with throughput gains of up to 2.3 times over previous work. The insights gained from the performance study not only advance the understanding of GPU-based joins but also introduce a structured approach to selecting the most efficient GPU join algorithm based on the input relation characteristics.

PVLDB Reference Format:

Bowen Wu, Dimitrios Koutsoukos, and Gustavo Alonso. Efficiently Processing Large Relational Joins on GPUs. PVLDB, 17(1): XXX-XXX, 2024. doi:XX.XX/XXX.XX

PVLDB Artifact Availability:

The source code, data, and/or other artifacts have been made available at <https://github.com/BowenforGit/GPU-Joins-Evaluation>.

1 INTRODUCTION

Nowadays, data centers need to process an ever-increasing amount of data emerging from applications such as Machine/Deep Learning (ML/DL), real-time data analytics, and databases. The increasing demands on computing, together with the end of Moore’s law, have made accelerators very popular [23, 62]. This is true, especially for GPUs, as they are highly effective in performing arithmetic operations, an essential building block for all ML/DL applications.

This work is licensed under the Creative Commons BY-NC-ND 4.0 International License. Visit <https://creativecommons.org/licenses/by-nc-nd/4.0/> to view a copy of this license. For any use beyond those covered by this license, obtain permission by emailing info@vldb.org. Copyright is held by the owner/author(s). Publication rights licensed to the VLDB Endowment.

Proceedings of the VLDB Endowment, Vol. 17, No. 1 ISSN 2150-8097.
doi:XX.XX/XXX.XX

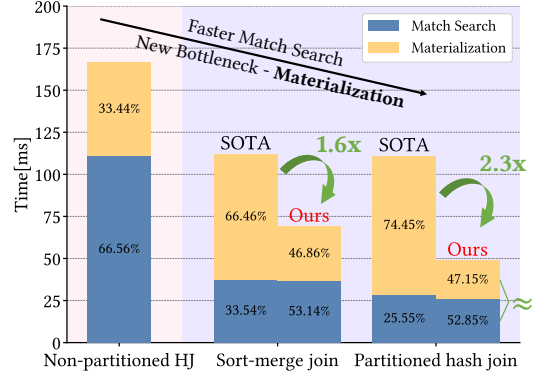


Figure 1: Time break-down for join processing.

Besides their effectiveness in arithmetic operations, GPUs have also orders of magnitude higher parallelism and memory bandwidth than CPUs [5, 15, 18], features that have attracted interest from database researchers and developers [13, 16, 21, 25, 30, 32, 34, 41, 42, 50, 53, 57, 66, 67]. This interest is reinforced by three trends. First, workloads, such as data pre-processing and ingestion for ML, often comprise of many different steps and run on CPUs and GPUs [68]. However, data transfer is one of the most expensive operations in data centers [22, 23] so it is advantageous to move relational operations to the GPU, where the final results will be processed as part of a downstream application, e.g., training an ML model. Second, the increased hardware capabilities of GPUs could potentially be used to accelerate costly relational operations like joins. And third, GPUs are now pervasive, with growing support in terms of development and tools. It makes sense to take advantage of these investments in hardware and software for relational operators as they are being done around, e.g., tensor computations [2, 47, 48].

The factors mentioned above, have triggered many efforts on optimizing relational operators in GPUs, especially joins [49, 55, 60, 65]. However, not all real-world settings have been studied in necessary detail. For instance, we analyzed two recent hardware-conscious join implementations on GPUs [55, 60] (Figure 1) by letting them join a primary-key relation of 1.5 GB with a foreign-key relation of 3 GB on an A100 GPU, each having two columns of payloads that need to be materialized. Although they are more efficient than the traditional non-partitioned hash join [21], the cost of materialization is very significant and can make up to 75% of the overall runtime. This is not entirely surprising since the same happens in a conventional CPU setting [1, 59]. The materialization cost is especially large for joins with a high match ratio and many non-key columns, a type of join common in both benchmarks (e.g., TPC-H, TPC-DS) and real-world scenarios. For example, with the rising popularity of in-database machine learning, it is common to perform joins without any filtering, which results in a 100% match

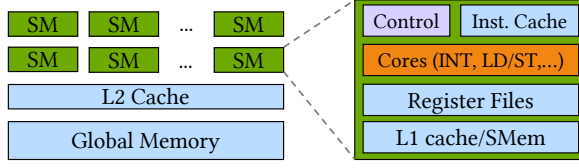


Figure 2: GPU architecture.

ratio [14, 37, 38]. This limitation of the state of the art is particularly relevant, e.g., when the relational join is part of an ML pipeline running on the GPU.

To better understand the role that GPUs could play in relational data processing, in this paper we present a comprehensive exploration of GPU-based join algorithms. We consider both *partitioned hash* and *sort-merge joins*, show how to optimize existing implementations, and systematically compare these two classes of join algorithms. Moreover, we study in detail the cost of materialization with examples from benchmarks and propose a widely applicable optimization technique, called “Gather-from-Transformed-Relations” (GFTR), to considerably improve performance for joins with expensive materialization. We extend our analysis with performance studies on microbenchmarks and TPC-H/DS benchmarks, which encompass a wider range of parameter settings and use cases, for example, sequences of joins, wider data types and keys, skewed distributions, different match ratios, and various input sizes.

The experimental evaluation shows that our optimization technique GFTR significantly improves performance for joins with high materialization costs while remaining competitive for low materialization cost. More specifically, our optimized join implementations are more than 20x faster than CPU implementations by Balkesen et al. [9] and up to 2.3x faster than previous GPU join implementations [60] (Figure 1). Besides processing joins with high materialization costs efficiently, we summarize the findings from the performance study into a set of simple yet highly practical heuristics for determining the best join algorithm under specific workloads, which is a valuable input to query optimizers for heterogeneous architectures.

2 BACKGROUND

2.1 General Purpose GPUs and CUDA

In this section, we briefly introduce the internals of GPUs and their hardware architecture. We also detail how NVIDIA’s Compute Unified Device Architecture (CUDA) works, and finally, we dive into optimization techniques for CUDA GPU programs.

In Figure 2, we present the high-level architecture of a GPU. The fundamental execution unit is the Streaming Multiprocessor (SM). Each SM consists of functional units that execute arithmetic and logic operations and memory loads/stores. Threads in an SM are grouped into *warps*. Warps consist of 32 threads working in a single-instruction-multiple-threads (SIMT) manner. In programs, threads are arranged into *thread blocks*, consisting of multiple warps that can share data over the fast on-chip memory and synchronize.

Each scheduled thread has its exclusive register files. Each SM shares an L1 cache. Part of the L1 cache can be configured as *shared memory*, which allows data sharing within a thread block. Developers can programmatically cache frequently used data in the shared memory to reduce global memory accesses. Further, all SMs share

a larger on-chip L2 cache. Finally, the global memory is the main storage for data on the GPU with a capacity varying from around 10 to more than 100 GB.

Efficient memory accesses are crucial for performance. In CUDA, memory accesses are most efficient when they are *coalesced*, i.e., when threads in a warp access consecutive memory locations. This allows the GPU to combine memory accesses into a single transaction. Uncoalesced or random accesses degrade performance significantly. When a warp is not ready for the next instruction (e.g., waiting for data from memory), it is stalled. When a warp is stalled, the scheduler switches to another warp ready to execute. This *latency hiding* technique ensures that throughput is maximized. However, it can only mitigate memory stalls to a limited extent – extensive irregular memory accesses can stall all warps, with the scheduler not being able to proceed. Therefore, to maximize performance, developers typically avoid random memory accesses and schedule data processing into continuous memory regions so that the GPU scheduler can always pick an active warp, thereby increasing parallelism.

2.2 In-memory Joins on GPUs

We now discuss a generic framework for GPU-based in-memory join algorithms and the assumptions that have been made in previous work [49, 55, 60, 65]. A join algorithm takes as input two relations, $R(k, r_1, \dots, r_n)$ and $S(k, s_1, \dots, s_m)$, and produces an output relation, $T(k, r_1, \dots, r_n, s_1, \dots, s_m)$ and with k as the key and $r_1, \dots, r_n, s_1, \dots, s_m$ as *payload* columns or non-key attributes. Each tuple can be uniquely identified by a physical or a virtual identifier. Physical IDs are stored as a column in the memory, whereas virtual IDs are inferred from tuple positions and not explicitly stored.

We distinguish the phases of the GPU join algorithm based on the number of payload columns of each input relation. In case there is only one payload column per relation, the join is a “narrow” join. The “narrow” join consists of two phases: 1) the transformation phase, where we transform R and S (for example by sorting or partitioning) into intermediate relations $R'(key, r_1)$ and $S'(key, s_1)$ and 2) the matching finding phase where we produce $T(key, r_1, s_1)$.

When the input relations have more than one payload column, it is a “wide” join. Processing a wide join is often simplified by turning it into a narrow join. This is done by generating the tuple identifiers for R and S , namely ID_R and ID_S . Then the join is done over $R(key, ID_R)$ and $S(key, ID_S)$. Subsequently, there is a materialization phase, using matching tuple IDs to copy the original payload values of each relation to the output. As a result, a wide join encompasses three phases. The first two are identical to the narrow join, and the last one is the materialization phase. The use of generated tuple identifiers simplifies the implementation of the match-finding process, and it is used by most GPU implementations [21, 32, 34, 49, 55, 60]. We follow the same approach.

Two common join algorithms are sort-merge and hash joins [26]. The sort-merge join first sorts the key attributes and then traverses the keys of both relations finding common matches [4, 36]. The hash join builds a hash table from usually the smaller relation and then probes this hash table using the second relation to find common keys [8, 12]. One very common optimization that has been proposed is partitioning [45, 58]. Partitioning divides the keys into smaller

chunks so that matches can only be found between co-partitions. Partitions are made sufficiently small to fit into the processor’s cache where random accesses are significantly faster. On the CPU, it is generally believed that the partitioned hash join performs better than sort-merge join [7]. In contrast, on the GPU, no systematic comparison has been made between these two algorithms.

2.3 GPU Primitives

We describe GPU *primitives*, which are procedures frequently present across many applications. These primitives, developed by GPU manufacturers [17, 20], provide high-performance out-of-the-box and are tuned automatically for different NVIDIA GPUs. The primitives used in this paper are the following:

- **RADIX-PARTITION**($kin, vin, kout, vout, i, j$). Partitions the key (kin) and value (vin) arrays, based on the radix bits of keys (i.e., the i -th to j -th bit in the binary representation). It stores the results in $kout$ and $vout$ arrays. In the result arrays, partitions are consecutively stored, making $kout$ ($vout$) the same size as kin (vin). For Ampere architecture, a maximum of 256 partitions (i.e., using max. 8 radix bits) can be produced by this primitive. To produce more than 256 partitions, we must invoke this primitive multiple times.
- **SORT-PAIRS**($kin, vin, kout, vout$). Sorts the kin, vin arrays pairs according to kin (i.e., keys) and produces $kouts, vouts$ arrays. Currently, the most efficient implementation for lexicographically comparable keys is the radix sort implemented by the CUB library [17], which internally uses RADIX-PARTITION.
- **GATHER**(in, map, out). For all valid i ’s, this primitive computes: $out[i] \leftarrow in[map[i]]$. Reading in may cause random memory accesses if the gather map map lacks “ordering” [29]. Depending on the efficiency of reading in , a *clustered* gather exhibits a low cache miss rate and highly coalesced memory accesses, compared to an *unclustered* gather that exhibits the opposite. We use this procedure in the materialization of payload columns.

3 STATE-OF-THE-ART GPU-ACCELERATED JOIN IMPLEMENTATIONS

In this section, we analyze the state-of-the-art GPU-based implementations of sort-merge and hash join. Our analysis shows that the existing implementations are only optimized for “narrow” joins while performing poorly for “wide” joins with a high match ratio.

Physically, relations are stored in the GPU memory as columns, and all columns are stored as arrays. This also applies to the output relation T . For the rest of this section, we analyze the “wide” join implementations. As introduced in Section 2.2, the “wide” join shares the same first two phases (transformation and match finding) as the “narrow” join.

3.1 Sort-Merge Join

In the transformation phase, the algorithm first initializes the *physical* tuple identifiers ID_R and ID_S for R and S and then sorts the pairs of columns, ($R.key, ID_R$) and ($S.key, ID_S$), to produce intermediate relations R' and S' , respectively. During sorting, we use the SORT-PAIRS primitive.

The match-finding phase identifies matching tuples between the sorted R' and S' . This phase produces the intermediate relation T' (key, ID_R, ID_S), which contains keys and IDs of matching

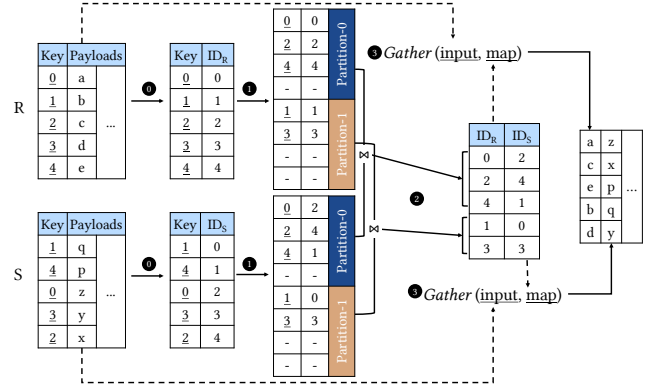


Figure 3: Partitioned hash join proposed by Sioulas et al.

tuples. To efficiently merge data on the GPU, Rui et al. [55] and ModernGPU [11] use the Merge Path algorithm [28]. This algorithm divides both R' and S' into non-overlapping partitions, where each partition pair is assigned to a GPU thread. The algorithm ensures that the partition pairs can be merged independently. It also guarantees that threads get approximately the same amount of work regardless of data distribution, which makes this algorithm resilient to data skewness. Both Rui et al. and ModernGPU apply the Merge Path algorithm twice: once to find the lower bound of each key of S' in R' , and a second time to determine the upper bound. The matches for a key in S' fall within the range defined by these two bounds. However, in a primary-foreign key join, a foreign key can have at most one matching primary key. In such a case, we only need to apply the Merge Path algorithm once to find either upper or lower bounds.

In the materialization phase, the ID_R and ID_S from T' are used to fetch matching tuple payloads from R and S and copy these values into the corresponding columns of the final output T . The process is repeated for all payload columns in both input relations using the GATHER primitive. However, ID_R and ID_S represent tuple IDs from *unsorted* relations. Thus, when sorting the relations during the transformation phase, they become randomly permuted. As a result, the GATHER operations in the materialization phase become unclustered, leading to a significant increase in uncoalesced memory accesses and cache misses.

3.2 Partitioned Hash Join

In the transformation phase, the partitioned hash join algorithm begins with initializing the *physical* tuple identifiers, ID_R and ID_S , for the relations R and S . It then proceeds to partition pairs of columns, namely ($R.key, ID_R$) and ($S.key, ID_S$), resulting in the intermediate relations R' and S' . Sioulas et al. [60] introduced a multi-pass radix partitioning implementation (Figure 3), which utilizes bucket chains to store and manage partitions. In this implementation, a bucket is a physically fixed-size, pre-allocated memory region, and it exclusively belongs to a single partition. Buckets within the same partition are connected through a chain, and each bucket maintains the location information of the next bucket in the chain.

During the partitioning phase, the algorithm allocates an initial bucket for each partition. If a partition’s size exceeds the capacity of a single bucket, new buckets are dynamically allocated and added

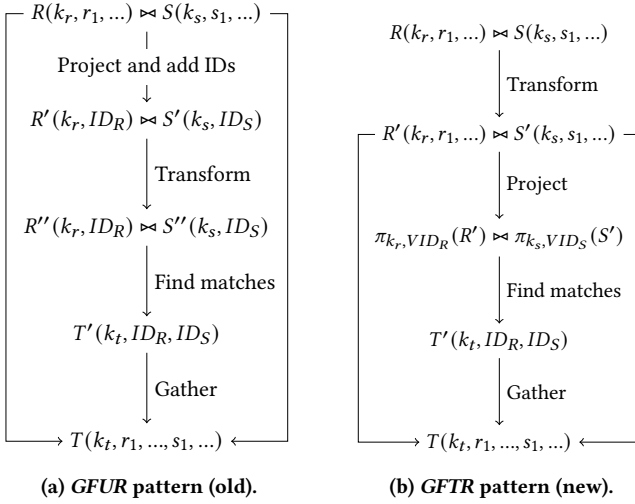


Figure 4: Comparison of two join implementation patterns.

to the chain. Although all buckets are allocated by “offsetting” a pre-allocated buffer, empty memory space exists between buckets since not all buckets are fully utilized.

For example, in Figure 3 the partition 0 cannot fill the entire bucket, and therefore, a gap exists between partition 0 and 1, leading to memory *fragmentation*. While partitioning, each thread block constructs a histogram in the shared memory for its work set using the radix bits. Subsequently, all thread blocks use atomic operations to determine the partition sizes and the locations to write the partitions. The partitioning requires multiple passes because large relations need a high fan-out to keep each partition sufficiently small such that it fits in the shared memory of an SM.

Partitioning with bucket chaining performs well because it leverages the shared memory and uses atomic operations to determine where each key should be written. Despite its high performance, the use of atomic operations can result in *non-deterministic* behavior [3], i.e., partitioning produces different outcomes across different runs. This occurs because the algorithm does not calculate prefix sums to decide where to write each tuple inside a partition; instead, a tuple is written when the thread has finished processing it.

Before the match-finding phase, Sioulas et al. balance the workloads among thread blocks. They decompose large probe-side partitions with many buckets into sub-partitions of fewer buckets. Then, they proceed to join co-partitions as follows: a thread block reads a bucket from the build-side partition, builds a hash table with it in the shared memory, and then probes the hash table with keys streaming from the probe-side partition. If a build-side partition has more than one bucket, they repeat the aforementioned procedure for each build-side bucket, in an operation resembling a block nested loop join. The hash join is highly efficient because the hash tables reside in the shared memory, and that reduces random accesses into the global memory.

The materialization process in partitioned hash join resembles that of sort-merge join. The GATHER is still unclustered, since the tuple identifiers, ID_R and ID_S , correspond to tuples in the original, non-partitioned input relations, which have been permuted due to the partitioning process.

3.3 Materialization Bottleneck

From the explanation of two state-of-the-art join implementations on the GPU, we observe that instead of optimizing the join of $R(k, r_1, \dots, r_n)$ and $S(k, s_1, \dots, s_m)$, they both focus on the efficient join of the transformed $R'(key, ID_R)$ and $S'(key, ID_S)$, namely the “narrow” join. During the materialization phase, they use inefficient unclustered GATHER procedures, because tuple IDs are randomly permuted as they transform their input relations. The optimization of the materialization phase is largely overlooked because it is regarded as a common cost to all implementations. In Figure 1, we have shown that although the sort-merge join and partitioned hash join have significantly improved the match search efficiency compared to the non-partitioned hash join, their materialization cost increases and emerges as a new bottleneck, which can take up around 75% of the execution time for a join operation.

4 OPTIMIZED JOIN IMPLEMENTATIONS

In this section, we introduce our optimized sort-merge and partitioned hash join algorithms with significantly improved materialization performance.

4.1 Co-design of All Join Phases

The sort-merge join and partitioned hash joins discussed in Section 3 follow the pattern depicted in Figure 4a. More specifically, the algorithm begins with associating keys of both relations, $R(k_r, r_1, \dots)$ and $S(k_s, s_1, \dots)$ with physical tuple identifiers, ID_R and ID_S , and produces relations of only two columns, namely $R'(k_r, ID_R)$ and $S'(k_s, ID_S)$. Afterwards, it partitions or sorts these relations producing $R''(k_r, ID_R)$ and $S''(k_s, ID_S)$. The algorithm then computes the matching tuples based on the selected algorithm (merge or hash join) and produces the output relation $T'(k_t, ID_R, ID_S)$, which contains the matched keys and tuple identifiers. Lastly, it uses ID_R and ID_S as gather maps to gather values from the non-key attributes of R and S . The greatest inefficiency of these implementations comes from the excessive random accesses of the GATHER primitives used in materialization. Due to partitioning or sorting, R'' , S'' contain random permutations of ID_R and ID_S that are highly unclustered. A warp that executes the GATHER primitive cannot coalesce the memory accesses to load $in[map[i]]$ and $in[map[i + 1]]$ or benefit from cache locality because these two values do not reside in the same cache line. Because the payload columns are not transformed together with the keys before gathering, we call this pattern “Gather-From-Untransformed-Relations” (GFUR).

We can improve GFUR by using the technique depicted in Figure 4b. In this new pattern, R and S are entirely transformed (either by sorting or by partitioning) into R' and S' . This means that we sort or partition *all* payload columns together with their key columns. After this step, we perform the join only for the key columns of R' and S' with their respective *virtual* tuple identifiers instead of physical ones. We materialize the virtual tuple identifiers VID_R, VID_S during the match-finding phase of the join, and use them to read payload values from R' and S' in the materialization phase. Note that VID_R of R' and VID_S of S' are sorted arrays, containing values from 0 to $|R| - 1$ or $|S| - 1$, as they represent tuple positions in the *transformed* input relations, R' and S' . This differs from the GFUR pattern, where ID_R of R' and ID_S of S' correspond to tuple

Algorithm 1: Actual implementation of GFTR pattern

Input: $R(k, r_1, \dots, r_n), S(k, s_1, \dots, s_m)$

Output: $T(k, r_1, \dots, r_n, s_1, \dots, s_m)$

► Transformation phase

1 $tk_r, tr_1 \leftarrow \text{transform}(R.k, R.r_1);$

2 $tk_s, ts_1 \leftarrow \text{transform}(S.k, S.s_1);$

► Match finding phase

3 $T.k, ID_R, ID_S \leftarrow \text{find-match}(tk_r, tk_s);$

► Materialization phase

4 **for** $i \leftarrow 1$ **to** n **do**

5 **if** $i > 1$ **then** $tk_r, tr_i \leftarrow \text{transform}(R.k, R.r_i);$

6 $T.r_i \leftarrow \text{gather}(tr_i, ID_R);$

7 **for** $i \leftarrow 1$ **to** m **do**

8 **if** $i > 1$ **then** $tk_s, ts_i \leftarrow \text{transform}(S.k, S.s_i);$

9 $T.s_i \leftarrow \text{gather}(ts_i, ID_S);$

positions of R and S . Knowing that VID_R and VID_S are clustered, it is equally important to guarantee that the ID_R and ID_S in T' (the output of the match finding) are also clustered; otherwise, the subsequent GATHERS will still be inefficient. Fortunately, the match-finding algorithms presented in this work, namely merge join and hash join, can produce clustered output tuple identifiers as long as the inputs themselves are clustered. This new pattern reduces the expensive random accesses during materialization by making the GATHER clustered. Because GATHER takes R' and S' as inputs, we call the pattern “Gather-From-Transformed-Relations” (GFTR).

We show the GFTR pattern implementation in Algorithm 1. In the transformation phase, we only transform the first payload column of R and S (Line 1-2). We postpone the transformation of other payload columns to the materialization phase right before the GATHERS (Line 4-9). This has two advantages. First, while we are transforming the first payload column of an input relation, we also transform the corresponding key column, which will be used for the match finding (Line 3). Second, transforming and gathering one payload column at a time saves memory because we do not store all transformed payload columns at once. The additional cost of GFTR is the transformation of entire input relations (from R to R' and S to S'). However, this transformation has a sequential memory access pattern, and thus, much faster than materialization. We show this to be the case in the experiments section. In the rest of this section, we show how to adapt the existing sort-merge and partitioned hash join algorithms to the GFTR pattern.

4.2 Optimized Sort-Merge Join

We show a high-level overview of the optimized sort-merge join in Figure 5. All payload columns are sorted with the corresponding keys (Step 1). We join keys together with *virtual* tuple identifiers (in gray) using the merge join (Step 2). Finally, we use the output tuple identifiers as maps to gather payload values from *sorted* payload columns (Step 3). The load instructions of GATHERS are coalesced with high probability because the ID_R and ID_S are clustered. Compared to the previous sort-merge join, the optimized version introduces the additional cost of sorting all payload columns. To sort a pair of 4-byte key column and 4-byte payload column, we

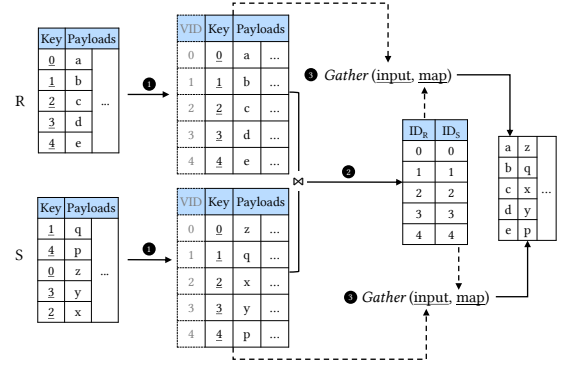


Figure 5: Optimized sort-merge join.

use the SORT-PAIRS primitive, which introduces about 17 sequential passes of key and payload arrays, because the SORT-PAIRS primitive is a least significant digit radix sort and sorts 8 radix bits at a time [3, 17]. During GATHER, the payload column is read sequentially once. In total, the optimized version sequentially scans (i.e., reads or writes) the key and payload columns about 18 times in order to replace the one random scan of the payload column in the unoptimized version. This might sound counter-intuitive but it exploits the huge performance gap between sequential and random memory access in GPUs.

4.3 Optimized Partitioned Hash Join

Given that the adaptation of the sort-merge join is straightforward, it is tempting to likewise adapt the existing partitioned hash join by partitioning all payload columns together with their keys. However, this optimization fails because of two properties of bucket-chain partitioning mentioned in Section 3.2, namely non-determinism and fragmentation. Firstly, during partitioning, a thread block uses *atomic* operations to allocate new buckets and determine where to write in the buckets. Atomic operations do not produce identical results across runs. For example, consider thread A and B both calling ATOMICADD on the OFFSET variable to determine at which positions they should write the output values. It is impossible to predict whether thread A’s output value appears before or after B’s because the order depends on which thread returns from the ATOMICADD first. Therefore, partitioning the pair (key, col_1) might have different results than partitioning (key, col_2) even though both are valid partitions. Non-determinism can lead to wrong join results. Additionally, even if we make the partitioning deterministic, the representation of partitions as chains of buckets makes it impossible to quickly look up values by indices in a partitioned column due to fragmentation. To access the i -th value in the partitioned payload column, we first need to calculate to which partition and which bucket it belongs to and the offset into that bucket. All these additional calculations make the materialization inefficient.

To apply the GFTR pattern in the partitioned hash join, we need to ensure that the partitioning produces consistent results across $(key, col_1), \dots, (key, col_n)$ and to look up values of a partitioned column by indices in constant time. To this end, we propose a new partitioned hash join implementation that overcomes these

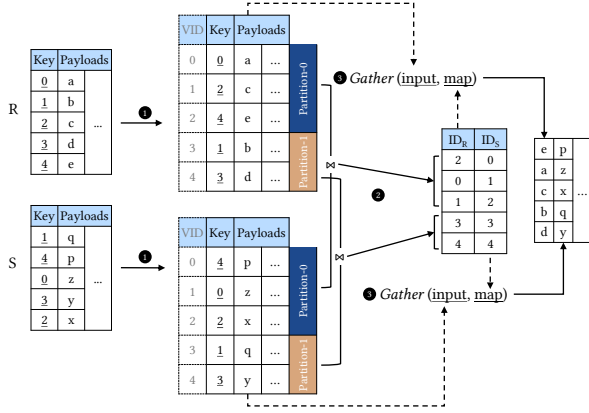


Figure 6: Optimized partitioned hash join.

difficulties (Figure 6). The partitioning phase (Step 1) uses the RADIX-PARTITION primitive to partition the input relations R and S into *contiguous* arrays, where values from the same partition are grouped together in the transformed relations R' and S' . Because the radix sort requires the RADIX-PARTITION to be stable [3], it will always produce the same partitioning results given the key column. That means that if k_1 occurs before k_2 in the input and they belong to the same partition, then k_1 should also occur before k_2 in the result.

Nonetheless, the boundaries between partitions are unknown after the radix partitioning. Thus, we need additional calculations to figure out the offset and size of each partition and we do so by constructing a histogram to find the size of each partition. Now that we know the partition size, we can determine the offset of each partition by calculating a prefix sum. To prevent partitions from being large and causing unbalanced workload distribution during the hash join, we re-partition them into smaller sub-partitions. Afterwards, in step 2 (Figure 6), we find the matches between the keys of R' and S' , after which identifiers of matched tuples are produced. Because the partitioned column is now an array instead of fragmented buckets, looking up by indices can be done in constant time, and GATHERS become efficient (Step 3). The additional transformation cost of this optimized partitioned hash join is partitioning all non-key attributes. For partitioning, we use 15 or 16 radix bits to determine a partition, resulting in two invocations of RADIX-PARTITION per payload column. Compared to four invocations of RADIX-PARTITION in sorting, partitioning is more efficient.

Theoretically, the optimized partitioned hash join guarantees that only the matching tuple identifiers of the probe relation are highly clustered, whereas those of the build relation are not as clustered. In practice, gathering the payloads from the build relation is also greatly improved compared to the unoptimized version.

It is important to clarify that while we propose a new partitioned hash join implementation to support the GFTR pattern, the implementation itself is not limited to GFTR. This implementation is flexible enough to follow the GFUR pattern as well by not partitioning the payload columns. This flexibility makes it competitive for workloads where the GFUR pattern performs better, such as joins with a low match ratio.

Table 1: GFUR memory consumption.

Phase	Activity	Alloc on entry	Free on exit	Used mem after exit	Peak mem
Transform	Initialize ID_R and transform R'	$M_t + 3M_c$	$M_t + M_c$	$2M_c$	$M_t + 3M_c$
	Initialize ID_S and transform S'	$M_t + 3M_c$	$M_t + M_c$	$4M_c$	$M_t + 5M_c$
Find matches	Write matching IDs	$2M_c$	$4M_c$	$2M_c$	$6M_c$
Materialize	Materialize payloads	0	$2M_c$	0	$2M_c$

4.4 Memory Consumption

In this section, we investigate if the GFTR pattern has a higher memory consumption than the GFUR pattern. A higher memory consumption would imply that the implementation would be limited to small joins since GPU main memory is scarce.

We compare these two patterns in their peak memory usage. Our analysis assumes that all columns and tuple IDs are of the same type, $|R| = |S| = |T|$, and the output relation is already allocated. We further assume that the memory for storing the input relations cannot be de-allocated. We denote the intermediate data (e.g., histograms) required by the transformation as M_t , and the memory space needed to store a column as M_c (e.g., physical IDs, transformed columns). The memory consumption of both patterns during execution is listed in Tables 1 and 2.

In the transformation phase, the GFTR achieves its peak memory consumption when we finish transforming R 's keys and its first payload column ($2M_c$ for transformed columns) and we allocate the memory for transforming S ($M_t + 2M_c$ for intermediate data and transformed columns). For GFUR, the transformation phase requires the initialization of physical tuple identifiers, ID_R and ID_S , giving a peak memory usage of $(M_t + 5M_c)$. After the transformation phase finishes, we can de-allocate M_t , ID_R , and ID_S . Thus, the allocated memory for both GFTR and GFUR is $4M_c$.

Right before the match-finding phase of both GFTR and GFUR, we allocate for each input relation an array to store the matching tuple IDs (i.e., ID_R and ID_S in T'). We write the matching keys directly to the output relation. Therefore, the peak memory consumption in the match-finding phase is $6M_c$ for both patterns, $4M_c$ of which is from the transformation phase. After match-finding, GFUR can release all memory allocated during the transformation phase whereas GFTR can only free the transformed keys but not the transformed payload columns. Therefore, at the end of this phase, GFUR and GFTR consume $2M_c$ and $4M_c$ of memory, respectively.

Finally, in the materialization phase, GFUR no longer allocates memory. For GFTR, we need an additional $M_t + 2M_c$ memory for transforming a payload column, before we materialize. That excludes the two payload columns already transformed in the transformation phase. The peak memory consumption for this phase is $2M_c$ (matching tuple IDs) + $M_t + 2M_c$ for GFTR and $2M_c$ (from the match-finding phase) for GFUR.

From the analysis above, it is evident that, in theory, the GFTR pattern is more memory-efficient than the GFUR, and implementations following the GFTR pattern can process problem sizes as large as those following the GFUR pattern. Therefore, the GFTR

Table 2: GFTR memory consumption.

Phase	Activity	Alloc on entry	Free on exit	Used mem after exit	Peak mem
Transform	(R) Transform keys w/ a non-key	$M_t + 2M_c$	M_t	$2M_c$	$M_t + 2M_c$
	(S) Transform keys w/ a non-key	$M_t + 2M_c$	M_t	$4M_c$	$M_t + 4M_c$
Find matches	Write matching IDs	$2M_c$	$2M_c$	$4M_c$	$6M_c$
Materialize	Materialize two already transformed payload columns	0	$2M_c$	$2M_c$	$4M_c$
	Materialize a not yet transformed payload column	$M_t + 2M_c$	$M_t + M_c$	$2M_c$	$M_t + 4M_c$

pattern does not limit the solvable problem scale given the same GPU memory capacity.

5 EXPERIMENTAL EVALUATION

5.1 Setup

Machine Configurations. We evaluate the existing and our optimized join implementations on two different machines with configurations detailed in Table 3. Both GPUs are based on the Ampere architecture and run CUDA version 12.2. The A100 GPU has more streaming multiprocessors, a larger L1 and L2 cache, and a higher memory bandwidth than the RTX 3090. Unless specified otherwise, we discuss and analyze results obtained from the A100 GPU, which is commonly found in data centers [6, 27, 56]. In cases where the results from the two GPUs diverge or the comparison is informative, we also discuss results from the RTX 3090.

Workload Description. We study the in-memory inner equi-join of two relations R and S on the GPU. We focus mostly on the primary-foreign key join as this is most commonly seen in queries [63, 64]. In this context, we assume that R holds the primary keys, and S holds the foreign keys. By default, we assume the keys and payloads in both relations are all 4-byte integers. In one of our experiments, we evaluate the performance when keys and payloads are 8-byte long. With the notation $1G \bowtie 2G$, we mean that we join two relations whose total sizes are 1 GB and 2 GB respectively, including payloads. We generate keys that take values from 0 to $|R| - 1$ and we randomly shuffle them.

Measurements. We evaluate the performance both in execution time and throughput. Following previous work [8, 44, 60], the

Table 3: Machine configurations.

	RTX 3090 Machine	A100 Machine
Compute capability	8.6	8.0
Streaming multiprocessors	82	108
L1 cache	128 KB	192 KB
Max. shared memory	100 KB	164 KB
L2 cache	6 MB	40 MB
Global memory	24 GB	40 GB
Theoretical memory bandwidth	936 GB/s	1,555 GB/s
Clock frequency	1,395 MHz	1,095 MHz

Table 4: Micro-architectural comparison between unclustered and clustered GATHERS on A100.

	Unclustered GATHER (in SMJ-UM)	Clustered GATHER (in SMJ-OM)
Number of items	2^{27}	2^{27}
Total cycles	12,052,942	1,414,398
Number of warp instructions	77,594,624	77,594,624
Avg. cycles per warp instruction	1037.06	115.74
Memory reads (in size)	4.5 GB	1.5 GB
Avg. sectors read per load request	18	6

throughput of a join is defined by $\frac{|R|+|S|}{\text{total time}}$. The total time measured only covers the join processing and does not include most memory allocations and initialization of auxiliary data structures. All experiments are repeated seven times, and we report the median.

In the measurements, we often report the time spent in each of the three join phases (transformation, match finding, and materialization). As explained in Section 4.1, the transformation and materialization phase in our optimized SMJ and PHJ overlap – the first payload column of each relation is transformed with the keys in the transformation phase. The remaining payload columns are transformed in the materialization phase. The time measured for each phase corresponds to the scope defined in Algorithm 1.

Implementations. We evaluate the performance of the following algorithms:

SMJ-UM (SU) Sort Merge Join with unoptimized materialization following the GFUR pattern (Section 3.1).

PHJ-UM (PU) Partitioned hash join with unoptimized materialization following the GFUR pattern (Section 3.2).

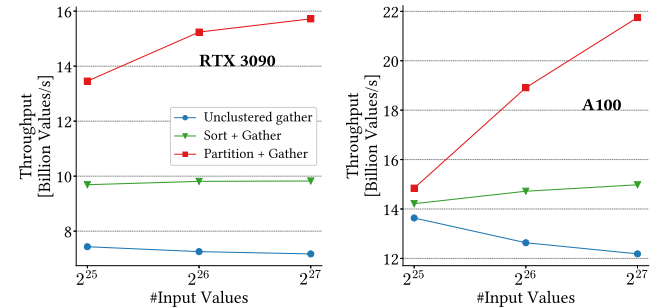
SMJ-OM (SO) Sort Merge Join with optimized materialization following the GFTR pattern (Section 4.2) proposed by us.

PHJ-OM (PO) Partitioned hash join with optimized materialization following the GFTR pattern (Section 4.3) proposed by us.

Finally, we also use wildcards to represent a class of implementations. For example, “SMJ-*” refers to sort-merge join implementations with or without optimized materialization, and “*-OM” covers any implementations with optimized materialization.

5.2 Microbenchmarks

We start our evaluation with microbenchmarks to assess the performance of various algorithms.


Figure 7: Comparison of efficiency between the unclustered GATHER and clustered GATHER with additional costs.

5.2.1 Clustered vs. Unclustered GATHER. In the first experiment we check how transforming all columns by sorting or partitioning before any GATHER alters performance. As explained in Section 4, the GATHER primitive is used in the materialization phase to write payload columns of matching tuples into the output relation. Gathering from transformed columns increases the probability that threads in a warp read payload values from the same cache line.

We first profile the GATHER primitive when performing a $1\text{G} \bowtie 1\text{G}$ join on A100. Table 4 shows the profiling results obtained from the NVIDIA Nsight Compute profiler [19]. Unclustered and clustered GATHER operations exhibit significant performance differences. Even though they execute the same number of warp instructions, the clustered GATHER is approximately 8.5 times faster than the unclustered GATHER. This gap arises from high memory access latency at the warp level, primarily due to uncoalesced accesses and low L2 cache hit rate. On average, when using the unclustered GATHER, a load instruction executed by a warp, results in loading 4.5 cache lines, opposed to just 1.5 cache lines with the clustered GATHER. Next, we examine the differences in performance between these two GATHER operations with the added cost of sorting or partitioning. Figure 7 shows the throughput of GATHERS used in *-UM, SMJ-OM, and PHJ-OM. Even with the sorting and partitioning overhead, the clustered GATHER outperforms the unclustered GATHER on both RTX 3090 and A100. On A100, partitioning and a clustered GATHER are 1.79x faster than an unclustered GATHER; on RTX 3090, they are 2.2x faster. For sorting and a clustered GATHER, the speedup is 1.23x and 1.37x for A100 and RTX 3090, respectively. Therefore, the GFTR pattern reduces the materialization cost despite the additional transformation cost. Note that a larger GPU like the A100 with a much larger L2 cache and higher memory bandwidth cannot alleviate the inefficiency of unclustered GATHERS.

5.2.2 Narrow and Wide Join Performance. We now compare the performance of narrow and wide joins with both optimized and unoptimized materialization. We first assume a match ratio of 100%, which means all tuples in S have a match partner in R . Moreover, S has twice as many tuples as R , namely $|S| = 2|R|$.

Figure 8 shows the throughput of the narrow join for different data sizes. The CPU join refers to the optimized radix join developed by Balkesen et al [9]. To have a fair comparison, we adjusted the CPU join implementation to run efficiently on our NUMA machine. cuDF join refers to the GPU-accelerated non-partitioned hash join implemented by cuDF [21]. The cuDF implementation does not include a transformation phase since R 's keys are directly inserted into a global hash table, which is then probed with S 's keys.

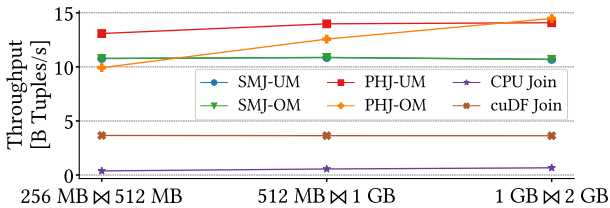


Figure 8: Comparison of CPU- and GPU-based narrow joins.

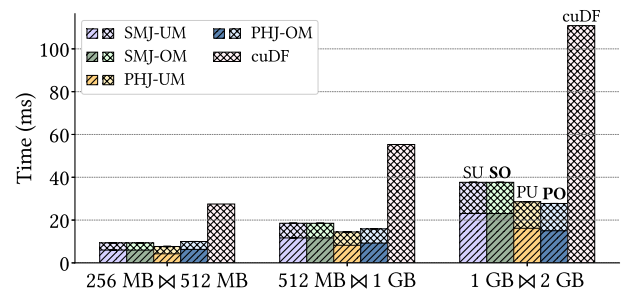


Figure 9: Time breakdown of narrow joins. (A bar corresponds to an implementation showing the transformation time (bottom) and match finding time (top).)

The match-finding phase in this case, includes the construction and probing of the hash table and the production of the matching tuple IDs. The materialization phase is identical to that of *-UM. As we see in the figure, the GPU-accelerated sort-merge join and partitioned hash join are up to 34.5 times faster than CPU joins and 4 times faster than the cuDF join. We also observe that PHJ-* perform better than SMJ-* for joining narrow tables. We depict the time breakdown of different GPU-based implementations for processing narrow joins in Figure 9. Since the joins are narrow, SMJ-OM is identical to SMJ-UM and performs worse than PHJ-*. PHJ-UM performs slightly better than PHJ-OM for smaller input sizes, yet both have almost identical performance for $1\text{G} \bowtie 2\text{G}$. Overall, the performance of PHJ-UM and PHJ-OM is very close. cuDF is the most inefficient of all because of the random accesses during the construction and probing of the hash table. To evaluate wide joins, we append to each relation two payload columns and we show the results in Figure 10. Even with two payload columns per relation, the materialization time dominates most *-UM implementations. Thus, implementations with optimized materialization have a significant advantage compared to the unoptimized implementations. More specifically, SMJ-OM is approximately 1.6x faster than SMJ-UM, and although sorting is considered costly, SMJ-OM achieves a 1.6x speedup over PHJ-UM. PHJ-OM stands out as the most performant algorithm, achieving around 2.3x and 1.4x better performance than PHJ-UM and SMJ-OM, respectively. It is better than SMJ-OM mainly because partitioning a column (or a pair of columns) needs 2 invocations of the RADIX-PARTITION (Section 4.3) primitive, whereas sorting needs

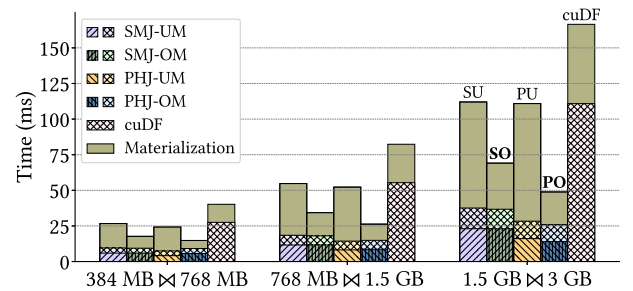


Figure 10: Time breakdown of wide joins.

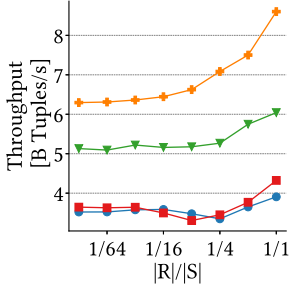


Figure 11: $|R|/|S|$.

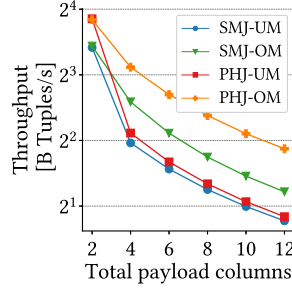


Figure 12: Payload columns.

four (Section 4.2). The non-partitioned hash join still performs the worst for the wide join case; however, it has a lower materialization cost than *-UM since materializing the probe table is clustered.

We evaluate two more factors that can affect the efficiency of wide joins. Figure 11 studies the relative size between R and S ($|S| = 2^{27}$). We observe that *-OM still outperform *-UM even though the materialization cost is lower when R is small. Additionally, figure 12 studies the effect of number of payload columns ($|R| = |S| = 2^{27}$). As the number of payload columns increases, PHJ-OM and SMJ-OM maintain 2x and 1.3x speedups over PHJ-UM, respectively.

5.2.3 Match Ratio. We now study the effect of different match ratios. With a high match ratio, more data are materialized, and therefore *-OM implementations perform better. On the other hand, a low match ratio, makes the materialization using unclustered GATHERS less costly, because only a small fraction of payload data are materialized. We adjust the match ratio by replacing a corresponding fraction of primary keys with non-matching values.

We show the effect of the match ratio in processing $1.5\text{G} \bowtie 1.5\text{G}$ in Figure 13 for relations R, S with two payload columns each ($|R| = |S| = 2^{27}$). We observe that *-OM implementations have better performance for high-match ratios, and when the ratio drops below 25%, *-OM are slower because the materialization is no longer a bottleneck. PHJ-UM has the best performance of all when the match ratio is low, due to the low materialization needs.

5.2.4 Data Skewness. Many datasets have a skewed foreign-key distribution which causes unbalanced workload distribution among execution units (e.g., thread blocks) during join processing. The unbalanced distribution reduces the level of parallelism by assigning a disproportionately large amount of the work to an execution unit. Following previous work [9], we generate the foreign key based on the Zipfian distribution and vary the Zipf factor to adjust the level of skewness. A high Zipf factor means that the data distribution is centralized at only a few values. Once again, R and S contain two payload columns each, and they both have a size of 1.5 GB ($|R| = |S| = 2^{27}$). We show the result of this experiment in Figure 14. As we observe in the figure, PHJ-UM is particularly sensitive to data skewness, with the partitioning cost increasing significantly as the Zipf factor grows and exceeds 1. This is mainly because of the uneven workload distribution among threads when allocating and bookkeeping the buckets in the first and second pass of partitioning, which leads to a high synchronization cost within a thread block.

This performance degradation indicates that the current bucket chaining implementation is unsuitable for non-uniform data, a bottleneck also found by Sioulas et al. [60].

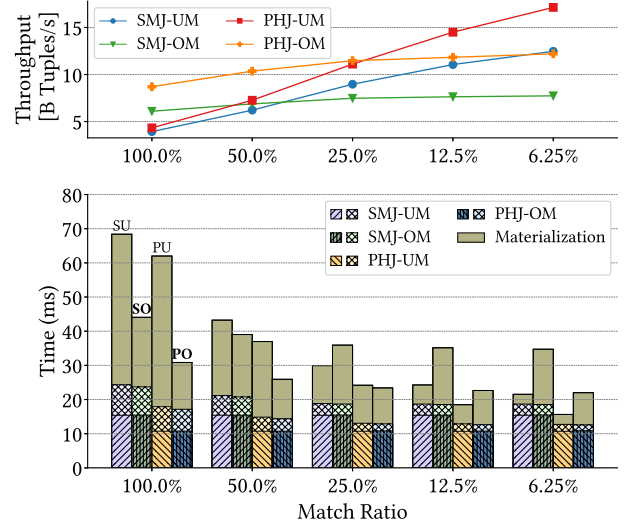


Figure 13: Effect of different match ratios.

On the other hand, the RADIX-PARTITION primitive used in PHJ-OM and SMJ-* is more robust to data skewness and exhibits consistent performance across all Zipf factors. RADIX-PARTITION ensures all threads get the same amount of work regardless of the data distribution. In all implementations, the match-finding phase is robust against data skewness, albeit for different reasons. In SMJ-*, the Merge Path algorithm helps balance the workload of each GPU thread. In PHJ-*, as discussed in Section 3.2 and 4.3, we perform a load-balancing step to decompose large partitions before the match-finding phase. As the foreign keys become increasingly skewed, the materialization cost is reduced because only a small portion of primary keys have matches. When the Zipf factor exceeds 1, SMJ-UM becomes more competitive due to its consistent sorting performance and lower materialization costs. In all cases, PHJ-OM has the best performance of all.

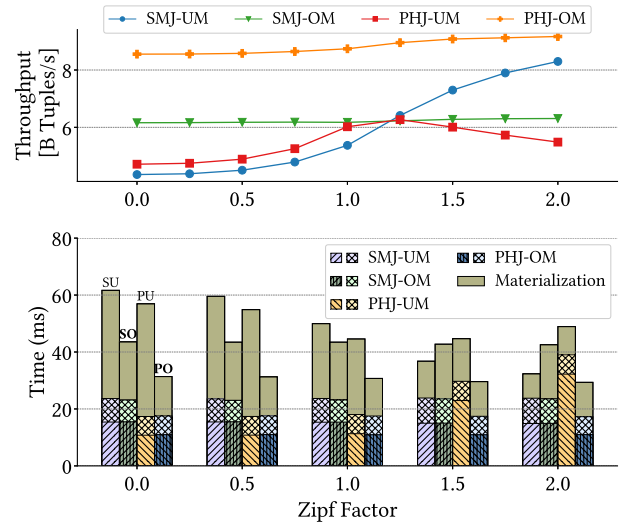


Figure 14: Effect of foreign key skewness.

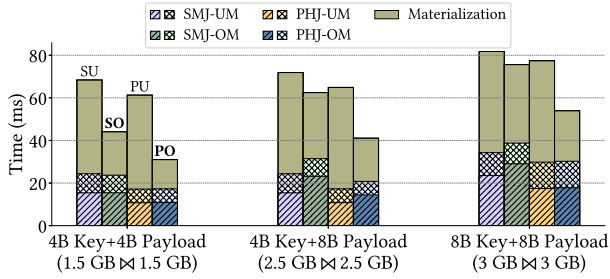


Figure 15: Effect of data types.

5.2.5 Data Types. Joins in the real world involve keys and payloads of various data types, whose sizes range from one byte to an arbitrary number of bytes (e.g., variable-length strings). Following previous work [8, 10], we evaluate the implementations with a mixture of 4-byte and 8-byte data. We let $|R| = |S| = 2^{27}$ tuples and we show the results in Figure 15. With the introduction of 8-byte values into payload columns (while keeping keys 4 bytes), *-UM maintains nearly the same performance as before, whereas *-OM experiences increased execution time due to more costly sorting and partitioning. Because of the high sorting cost, SMJ-OM becomes less superior to *-UM. In *-OM, the RADIX-PARTITION primitive reads and writes 4-byte keys and 8-byte payload values, whereas in *-UM, it handles 4-byte keys and 4-byte tuple identifiers regardless of the 8-byte payload values. When both keys and payload values are 8-bytes, the transformation and match-finding phase in all implementations become more expensive. SMJ-OM, in this case, has almost no advantage over *-UM. On the other hand, PHJ-OM leads the performance for all cases. Notably, when the size of keys and payloads increases, the materialization cost of *-UM methods remains nearly constant. This is because the unclustered GATHER is bound by memory access latency, and accessing 4-byte and 8-byte values causes accesses to a similar number of cache lines. For all combinations of data types examined here, PHJ-OM achieves the best performance.

5.2.6 Memory Consumption. We present the peak memory consumption for each implementation when processing workloads from the last section in Table 5. We aim to demonstrate that the performance advantage observed with our optimized implementations in microbenchmarks does not incur any additional memory overhead. The actual memory usage differs from the theoretical lower bound given in Section 4.4. That happens because we allocate the majority of the consumed memory before executing the join and only release it after the execution. This approach minimizes memory management overhead during the execution of the algorithm. Our experimental evaluation, shown in Table 5, proves that SMJ-OM and PHJ-OM, in all cases, are more memory efficient than SMJ-UM and PHJ-UM across all data types.

5.2.7 Sequences of joins. We investigate the efficiency of processing sequences of joins, similar to Bandle et al. [10]. To do so, we construct sequences of N joins, where the fact table F has N foreign keys (FK_1, \dots, FK_N), corresponding to dimension tables D_1, \dots, D_N . Each dimension table D_i consists of a primary key

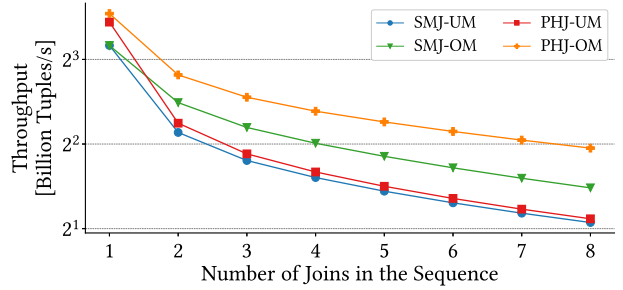


Figure 16: Sequences of joins

K_i and a payload column P_i . To minimize materialization, we initialize physical tuple identifiers for the fact table, which we use to fetch the relevant foreign key *right before* the corresponding join. This approach avoids unnecessary materialization of irrelevant foreign keys for each join operation. The i -th join processes ($FK_i, ID, P_1, \dots, P_{i-1}$) $\bowtie D_i$. Before the $(i+1)$ -th join, we utilize tuple IDs from the i -th join's result to materialize FK_{i+1} .

Figure 16 shows the results for $|F| = 2^{27}$ tuples and $|D_1| = \dots = |D_N| = 2^{25}$ tuples for an increasing number of joins. As we perform more joins, all implementations experience decreased throughput because each join needs to materialize one more column than the previous join. When the pipeline has more than two joins, *-OM outperforms *-UM, with the performance advantage growing as the sequence increases. For instance, PHJ-OM is 1.49 times faster than PHJ-UM for a sequence of two joins, and it is 1.78 times faster when we join 8 tables.

5.3 TPC-H/TPC-DS Queries

As a final experiment, we evaluate all implementations with five representative joins from the TPC-H [64] and TPC-DS [63] benchmarks, specified in Table 6. We extract these joins from the query plans produced by the DuckDB [52] query optimizer, and we pick them because they are more diversified than those in the microbenchmarks. For example, J4 has a large size difference between the input relations, J5 contains a self foreign-key join and all of the joins picked contain various numbers of payload columns.

Table 5: Memory usage

	4B Key + 4B Payload	4B Key + 8B Payload	8B Key + 8B Payload
SMJ-UM	11 G	15 G	20 G
SMJ-OM	9.5 G	15 G	18 G
PHJ-UM	12.6 G	16.6 G	21.1 G
PHJ-OM	9.5 G	15 G	18 G

Table 6: TPC-H/DS benchmark query specification.

Benchmark	ID	Query	$ R $	$ S $	$ R \bowtie S $	Payload cols	Remark
TPC-H (SF=10)	J1	Q7	15M	18.2M	18.2M	1K3NK(R)+1NK(S)	PK-FK wide join
	J2	Q18	15M	60M	60M	1K2NK(R)+1NK(S)	
	J3	Q19	2M	2.1M	2.1M	3NK(R)+3NK(S)	
TPC-DS (SF=100)	J4	Q64	1.9M	58M	58M	1NK(R)+3K7NK(S)	Self narrow join
	J5	Q95	72M	72M	904M	1NK(R)+1NK(S)	

For this experiment, the key attributes refer not only to join keys but also to any primary and foreign keys that may be contained in the input relations as payload columns. We summarize the number of key (“K”) and non-key (“NK”) attributes for each join in Table 6. Additionally, we transform strings into numeric values by dictionary encoding, and we randomly shuffle the rows of the input relations. In contrast to previous work that exclusively uses 4-byte data types for both key and non-key attributes, we use a mixture of 4-byte and 8-byte values to align with the benchmark specifications. We present the results of our experiment in Figure 17a.

We first let the key attributes be 4-bytes and non-key attributes to be 8-bytes. J1, J2, and J3 resemble the joins studied in Section 5.2.2 where $|S|$ and $|R|$ are close in size, and each relation only has 1–4 payload columns. For these three joins, *-OM perform almost always better, and their advantage is more pronounced when the input relations are large (i.e., J2). When the input relations are small, for example in J3, the GPU utilizes the L2 cache better making the unclustered GATHER faster. When the join involves many payload columns from the larger input relation (i.e., J4), PHJ-OM still greatly outperforms the other implementations, whereas SMJ-OM has a minor performance advantage. For SMJ-OM, the performance benefit of the clustered GATHERS is negligible or even reversed by the high cost of sorting 8-byte payload columns. J6 is a narrow join of foreign keys from the same relation producing an output relation that is 12x as large as either input relation. All implementations exhibit very close match-finding efficiency. However, since partitioning is more efficient than sorting, PHJ-* has the best performance in J6. Finally, PHJ-OM and PHJ-UM have nearly identical performance for J6 in both partitioning and match finding. We also let all attributes be 8-bytes, in which case the cost of sorting increases significantly. While SMJ-OM has better performance for joins with a moderate number of payload columns (J2), the advantage vanishes when the number of payload columns is very large (J4). When input relations

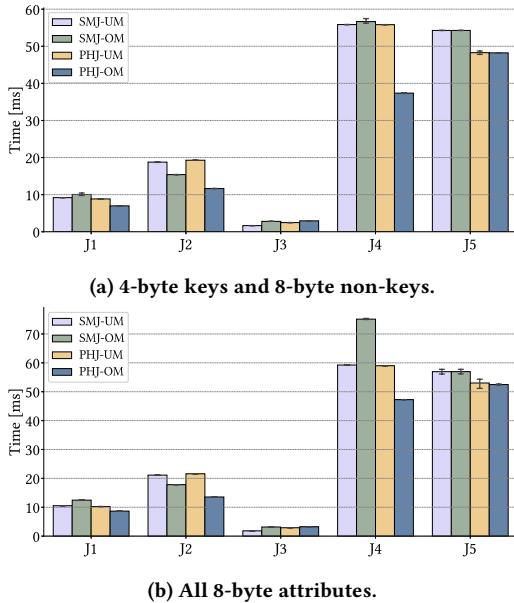


Figure 17: Joins from TPC-H and TPC-DS benchmarks.

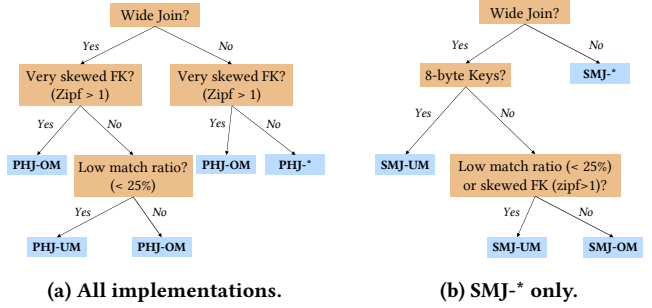


Figure 18: Decision trees.

are small and unclustered GATHERS are not very expensive (J1 and J3), SMJ-OM also does not have any performance advantage. On the other hand, PHJ-OM performs consistently well for all evaluated joins even though partitioning becomes more costly with the introduction of 8-byte values. These results show that for datasets having a high proportion of 8-byte values, the extra sorting cost of SMJ-OM does not pay off, whereas PHJ-OM consistently benefits from partitioning all payload columns.

5.4 Summary

From the microbenchmarks and TPC-H/DS evaluation, partitioned hash joins are superior to sort-merge joins for all cases. Based on the microbenchmarks, Figure 18a shows the decision tree to choose the best implementation out of all four implementations, and Figure 18b summarizes the comparison between SMJ-OM and SMJ-UM only. For narrow joins or wide joins with low match ratios, PHJ-* have better performance than SMJ-*, and PHJ-OM performs even better for skewed data due to more efficient partitioning. For wide joins, PHJ-OM and SMJ-UM are the best choices to deal with skewed foreign keys. If the foreign keys are more uniformly distributed, and materialization time dominates the overall runtime, *-OM is better in most cases. With the presence of 8-byte values in keys and/or payloads, SMJ-OM experiences performance degradation and loses its competitiveness to *-UM, whereas PHJ-OM maintains its superiority. The reason that partitioned hash join variants dominate the algorithm choice in all scenarios is because partitioning is more efficient than sorting but both transformations make the match-finding phase similarly efficient.

TPC-H/DS benchmarks are much more complex than those studied in microbenchmarks, and hence it is highly non-trivial to predict the optimal implementation for a certain join. To be more capable of predicting the best implementation given input relations, it is crucial to profile the primitives (Section 2.3) beforehand under different setups (such as machines, input sizes, and data distribution) since they have the greatest impact on the performance. To decide if we should use implementations based on the GFTR pattern (namely *-OM), we can use the profiler results to weigh clustered GATHERS with additional transformation cost against unclustered GATHERS. From our experiment study, we observe that that SMJ-OM is efficient when the joins keys are 4-byte, and the payload columns are mostly 4-bytes, whereas PHJ-OM is advantageous for all cases as long as the match ratio is sufficiently high. This type of information is typically available to an optimizer, which can use these guidelines to select the best join operator.

6 RELATED WORK

GPU-based Joins. Rui et al. [55] designed partitioned radix joins and sort-merge joins for GPUs by utilizing new hardware features, such as atomics, larger register files, and shared memory. They focused on the speedup of the GPU-based implementations relative to the CPU-based without comparing these two GPU-based algorithms across various workloads. Their proposed two-pass radix partitioning algorithm constructs a histogram per thread block in shared memory and then uses a prefix scan across all histograms to determine the position of each partition. However, their approach requires a separate kernel invocation for the prefix scan, resulting in reloading of data from global memory when resuming the partitioning. In contrast, the RADIX-PARTITION primitive used in this work computes the prefix scan in the same kernel as the histogram construction, using the OneSweep technique [3]. Sioulas et al. [60] proposed another partitioning algorithm using bucket-chaining, which also avoids the inefficient prefix scan using atomics to determine the output positions. Paul et al. [49] revisited multiple hash joins on the GPUs and concluded that the partitioned hash join proposed by Sioulas et al. [60] outperforms all other existing hash join implementations. Our newly proposed partitioned hash join (PHJ-OM) achieves the same partition efficiency, while fixing the fragmentation and non-determinism issues. In addition, the optimized version performs significantly better as the materialization cost grows. More recently, some GPU-based query engines are adopting tensor operations to implement relational operators, like joins. He et al. [32] implemented the sort- and hash-based joins using tensor operations in their Tensor Query Processor (TQP). Hu et al. [34] converted joins to matrix multiplications, which can then be computed efficiently using the Tensor Core Units. However, the main focus of these efforts is not on joins but on building a complete query engine, and hence they do not optimize the join operator. Sun et al. [61] showed that both tensor-based joins have worse performance than cuDF and the partitioned hash join from [60]. The joins proposed in this paper outperform the latter, thus justifying the choice of baselines we have made. Different from all previous methods, Doraiswamy et al. [24] leverage the graphics pipeline architecture instead of CUDA programming to implement a hardware-agnostic join. However, this work, alongside all previous work listed above, only optimizes for the narrow joins without considering materialization cost, which takes up the majority of the join execution time, as shown in the introduction.

A variety of other join implementations have been proposed and studied for older GPUs [31], multi-way joins [40], CPU-GPU co-processing [33, 60], out-of-memory cases [35, 55, 60], multi-GPUs [51, 54], fast interconnects [43, 44], or as part of a GPU-based query engines [13, 21, 30, 57]. Our method is orthogonal to these techniques, as we concentrate only on joins on a single GPU.

Materialization. Materialization strategies have been extensively explored in the context of CPU-based joins within column-oriented database systems. Ababi et al. [1] compared the early and late materialization of the inner table (i.e., build table in hash join) when processing wide joins. They found that early materialization is more efficient when the match ratio of the join is high. The GFTR pattern,

proposed in this work, can be viewed as a revised version of early materialization for GPU-based joins. In early materialization, we reconstruct the columns into rows before the join and transform the rows in the transformation phase. In GFTR, we skip the row reconstruction and transform the columns *one by one*. The effect is the same – all payloads are transformed and the materialization is therefore faster. In the meantime, GFTR is more efficient in memory consumption than early materialization because 1) reconstructed rows and *all* original columns will co-exist during the reconstruction; and 2) transforming wide rows consumes more memory than transforming a narrow column. Additionally, Shrinivas et al. [59] and Bandle et al. [10] demonstrated that early materialization, enhanced with sideways information passing, can be more efficient than late materialization for low match-ratio joins. However, our work focuses on joins with a high match ratio. Finally, Manegold et al. [46] also observed that the unclustered GATHER (referred to as positional join in their work) is a dominant cost in joins with many columns. To address this, they proposed the radix decluster algorithm to optimize the late materialization of payload columns. This algorithm is proposed for single-thread execution, and therefore it is not suitable for GPUs.

GATHER Optimization. We have shown that unclustered GATHERs are the main source of inefficiency during materialization. There are also efforts trying to optimize this operation. He et al. [29] designed multi-pass gather operations to improve the cache locality and reported a 30%-50% performance improvement. Ten years later, Lai et al. [39] revisited the multi-pass technique and concluded that 1) TLB caching contributes more to the improved performance; and 2) more importantly, newer GPUs (Pascal GPUs and onwards) benefit little from the multi-pass technique because their TLBs have a much larger reach. Therefore, our work still adopts the single-pass gather implementation provided by the Thrust library [20].

7 CONCLUSION

In this paper, we have proposed a new optimization technique, called GFTR, to efficiently execute wide joins with high materialization costs on GPUs. Starting from previous state-of-the-art implementations, we identified how materialization can be the most expensive phase of the algorithm and analyzed why previous work was ineffective in materializing the output of joins. Based on these insights, we proposed GFTR to speed up the materialization of joins with an arbitrary number of non-key columns. We evaluated our new algorithm extensively under various scenarios, challenging various assumptions that previous work has made. Our experimental results prove the effectiveness of our approach, improving state-of-the-art GPU-based join algorithms up to 2.3 times and outperforming CPU-based joins by more than 20 times. Besides our performance improvements, we also make specific recommendations for query optimization on joins for GPUs.

ACKNOWLEDGMENTS

The research has been supported in part by a generous donation from Meta. We would like to thank Pedro Pedreira for input on Velox and the role of GPUs in relational data processing.

REFERENCES

- [1] Daniel J. Abadi, Daniel S. Myers, David J. DeWitt, and Samuel R. Madden. 2007. Materialization Strategies in a Column-Oriented DBMS. In *2007 IEEE 23rd International Conference on Data Engineering*. 466–475. <https://doi.org/10.1109/ICDE.2007.367892>
- [2] Martin Abadi, Ashish Agarwal, Paul Barham, Eugene Brevdo, Zhifeng Chen, Craig Citro, Greg S. Corrado, Andy Davis, Jeffrey Dean, Matthieu Devin, Sanjay Ghemawat, Ian Goodfellow, Andrew Harp, Geoffrey Irving, Michael Isard, Yangqing Jia, Rafal Jozefowicz, Lukasz Kaiser, Manjunath Kudlur, Josh Levenberg, Dandelion Mané, Rajat Monga, Sherry Moore, Derek Murray, Chris Olah, Mike Schuster, Jonathon Shlens, Benoit Steiner, Ilya Sutskever, Kunal Talwar, Paul Tucker, Vincent Vanhoucke, Vijay Vasudevan, Fernanda Viégas, Oriol Vinyals, Pete Warden, Martin Wattenberg, Martin Wicke, Yuan Yu, and Xiaoqiang Zheng. 2015. TensorFlow: Large-Scale Machine Learning on Heterogeneous Systems. <https://www.tensorflow.org/>. Software available from tensorflow.org.
- [3] Andy Adinets and Duane Merrill. 2022. Onesweep: A Faster Least Significant Digit Radix Sort for GPUs. arXiv:2206.01784 [cs.DC]
- [4] Martina-Cezara Albutiu, Alfons Kemper, and Thomas Neumann. 2012. Massively Parallel Sort-Merge Joins in Main Memory Multi-Core Database Systems. *Proc. VLDB Endow.* 5, 10 (jun 2012), 1064–1075. <https://doi.org/10.14778/2336664.2336678>
- [5] AMD. 2023. AMD Instinct MI250X Accelerator. <https://www.amd.com/en/products/server-accelerators/instinct-mi250x>
- [6] Azure. 2023. GPU optimized virtual machine sizes. online. <https://learn.microsoft.com/en-us/azure/virtual-machines/sizes-gpu>
- [7] Cagri Balkesen, Gustavo Alonso, Jens Teubner, and M. Tamer Özsu. 2013. Multi-Core, Main-Memory Joins: Sort vs. Hash Revisited. *Proc. VLDB Endow.* 7, 1 (sep 2013), 85–96. <https://doi.org/10.14778/2732219.2732227>
- [8] Cagri Balkesen, Jens Teubner, Gustavo Alonso, and M. Tamer Özsu. 2013. Main-memory hash joins on multi-core CPUs: Tuning to the underlying hardware. In *2013 IEEE 29th International Conference on Data Engineering (ICDE)*. 362–373. <https://doi.org/10.1109/ICDE.2013.6544839>
- [9] Cagri Balkesen, Jens Teubner, Gustavo Alonso, and M. Tamer Özsu. 2015. Main-Memory Hash Joins on Modern Processor Architectures. *IEEE Transactions on Knowledge and Data Engineering* 27, 7 (2015), 1754–1766. <https://doi.org/10.1109/TKDE.2014.2313874>
- [10] Maximilian Bandle, Jana Giceva, and Thomas Neumann. 2021. To Partition, or Not to Partition, That is the Join Question in a Real System. In *Proceedings of the 2021 International Conference on Management of Data (Virtual Event, China) (SIGMOD '21)*. Association for Computing Machinery, New York, NY, USA, 168–180. <https://doi.org/10.1145/3448016.3452831>
- [11] Sean Baxter. 2016. moderngpu 2.0. (2016). <https://github.com/moderngpu/moderngpu/wiki>
- [12] Spyros Blanas, Yanan Li, and Jignesh M. Patel. 2011. Design and Evaluation of Main Memory Hash Join Algorithms for Multi-Core CPUs. In *Proceedings of the 2011 ACM SIGMOD International Conference on Management of Data (Athens, Greece) (SIGMOD '11)*. Association for Computing Machinery, New York, NY, USA, 37–48. <https://doi.org/10.1145/1989323.1989328>
- [13] Sebastian Breß. 2014. The Design and Implementation of CoGaDB: A Column-oriented GPU-accelerated DBMS. *Datenbank-Spektrum* 14 (2014), 199 – 209. <https://api.semanticscholar.org/CorpusID:256060600>
- [14] Nadia Chepurko, Ryan Marcus, Emanuel Zraggen, Raul Castro Fernandez, Tim Kraska, and David Karger. 2020. ARDA: Automatic Relational Data Augmentation for Machine Learning. *Proc. VLDB Endow.* 13, 9 (may 2020), 1373–1387. <https://doi.org/10.14778/3397230.3397235>
- [15] Jack Choquette, Wishwesh Gandhi, Olivier Giroux, Nick Stam, and Ronny Krashinsky. 2021. NVIDIA A100 Tensor Core GPU: Performance and Innovation. *IEEE Micro* 41, 2 (2021), 29–35. <https://doi.org/10.1109/MM.2021.3061394>
- [16] Periklis Chrysogelos, Manos Karpasiotakis, Raja Appuswamy, and Anastasia Ailamaki. 2019. HetExchange: Encapsulating Heterogeneous CPU-GPU Parallelism in JIT Compiled Engines. *Proc. VLDB Endow.* 12, 5 (jan 2019), 544–556. <https://doi.org/10.14778/3303753.3303760>
- [17] NVIDIA Corporation. 2023. Cooperative primitives for CUDA C++. <https://github.com/NVIDIA/cub> GitHub repository.
- [18] NVIDIA Corporation. 2023. NVIDIA H100 Tensor Core GPU Architecture. <https://resources.nvidia.com/en-us-tensor-core>
- [19] NVIDIA Corporation. 2023. NVIDIA Night Compute. online. <https://developer.nvidia.com/nsight-compute>
- [20] NVIDIA Corporation. 2023. Thrust: Parallel Algorithms Library. <https://github.com/NVIDIA/thrust> GitHub repository.
- [21] RAPIDS cuDF Developers. 2023. cuDF: GPU DataFrame Library. <https://github.com/rapidsai/cudf> GitHub repository.
- [22] Bill Dally. 2011. Power, programmability, and granularity: The challenges of exascale computing. In *2011 IEEE International Test Conference*. IEEE Computer Society, 12–12.
- [23] William J Dally, Yatish Turakhia, and Song Han. 2020. Domain-specific hardware accelerators. *Commun. ACM* 63, 7 (2020), 48–57.
- [24] Harish Doraiswamy, Vikas Kalagi, Karthik Ramachandra, and Jayant R. Haritsa. 2023. A Case for Graphics-Driven Query Processing. *Proc. VLDB Endow.* 16, 10 (jun 2023), 2499–2511. <https://doi.org/10.14778/3603581.3603590>
- [25] Henning Funke, Sebastian Breß, Stefan Noll, Volker Markl, and Jens Teubner. 2018. Pipelined Query Processing in Coprocessor Environments. In *Proceedings of the 2018 International Conference on Management of Data (Houston, TX, USA) (SIGMOD '18)*. Association for Computing Machinery, New York, NY, USA, 1603–1618. <https://doi.org/10.1145/3183713.3183734>
- [26] Hector Garcia-Molina, Jeffrey D. Ullman, and Jennifer Widom. 2008. *Database Systems: The Complete Book* (2 ed.). Prentice Hall Press, USA.
- [27] Google. 2023. Google Cloud GPU Platforms. online. <https://cloud.google.com/compute/docs/gpus>
- [28] Oded Green, Robert McColl, and David A. Bader. 2012. GPU Merge Path: A GPU Merging Algorithm. In *Proceedings of the 26th ACM International Conference on Supercomputing (San Servolo Island, Venice, Italy) (ICS '12)*. Association for Computing Machinery, New York, NY, USA, 331–340. <https://doi.org/10.1145/2304576.2304621>
- [29] Bingsheng He, Naga K. Govindaraju, Qiong Luo, and Burton Smith. 2007. Efficient gather and scatter operations on graphics processors. In *SC '07: Proceedings of the 2007 ACM/IEEE Conference on Supercomputing*. 1–12. <https://doi.org/10.1145/1362622.1362684>
- [30] Bingsheng He, Mian Lu, Ke Yang, Rui Fang, Naga K. Govindaraju, Qiong Luo, and Pedro V. Sander. 2009. Relational Query Coprocessing on Graphics Processors. *ACM Trans. Database Syst.* 34, 4, Article 21 (dec 2009), 39 pages. <https://doi.org/10.1145/1620585.1620588>
- [31] Bingsheng He, Ke Yang, Rui Fang, Mian Lu, Naga Govindaraju, Qiong Luo, and Pedro Sander. 2008. Relational Joins on Graphics Processors. In *Proceedings of the 2008 ACM SIGMOD International Conference on Management of Data (Vancouver, Canada) (SIGMOD '08)*. Association for Computing Machinery, New York, NY, USA, 511–524. <https://doi.org/10.1145/1376616.1376670>
- [32] Dong He, Supun C Nakandala, Dalitso Banda, Rathijit Sen, Karla Saur, Kwanghyun Park, Carlo Curino, Jesús Camacho-Rodríguez, Konstantinos Karanasos, and Matteo Interlandi. 2022. Query Processing on Tensor Computation Runtimes. *Proc. VLDB Endow.* 15, 11 (jul 2022), 2811–2825. <https://doi.org/10.14778/3551793.3551833>
- [33] Jiong He, Mian Lu, and Bingsheng He. 2013. Revisiting Co-Processing for Hash Joins on the Coupled CPU-GPU Architecture. *Proc. VLDB Endow.* 6, 10 (aug 2013), 889–900. <https://doi.org/10.14778/2536206.2536216>
- [34] Yu-Ching Hu, Yuliang Li, and Hung-Wei Tseng. 2022. TCUDB: Accelerating Database with Tensor Processors. In *Proceedings of the 2022 International Conference on Management of Data (Philadelphia, PA, USA) (SIGMOD '22)*. Association for Computing Machinery, New York, NY, USA, 1360–1374. <https://doi.org/10.1145/3514221.3517869>
- [35] Tim Kaldewey, Guy Lohman, Rene Mueller, and Peter Volk. 2012. GPU Join Processing Revisited. In *Proceedings of the Eighth International Workshop on Data Management on New Hardware (Scottsdale, Arizona) (DaMoN '12)*. Association for Computing Machinery, New York, NY, USA, 55–62. <https://doi.org/10.1145/2236584.2236592>
- [36] Changkyu Kim, Tim Kaldewey, Victor W. Lee, Eric Sedlar, Anthony D. Nguyen, Nadathur Satish, Jatin Chhugani, Andrea Di Blas, and Pradeep Dubey. 2009. Sort vs. Hash Revisited: Fast Join Implementation on Modern Multi-Core CPUs. *Proc. VLDB Endow.* 2, 2 (aug 2009), 1378–1389. <https://doi.org/10.14778/1687553.1687564>
- [37] Arun Kumar, Jeffrey Naughton, and Jignesh M. Patel. 2015. Learning Generalized Linear Models Over Normalized Data. In *Proceedings of the 2015 ACM SIGMOD International Conference on Management of Data (Melbourne, Victoria, Australia) (SIGMOD '15)*. Association for Computing Machinery, New York, NY, USA, 1969–1984. <https://doi.org/10.1145/2723372.2723713>
- [38] Arun Kumar, Jeffrey Naughton, Jignesh M. Patel, and Xiaojin Zhu. 2016. To Join or Not to Join? Thinking Twice about Joins before Feature Selection. In *Proceedings of the 2016 International Conference on Management of Data (San Francisco, California, USA) (SIGMOD '16)*. Association for Computing Machinery, New York, NY, USA, 19–34. <https://doi.org/10.1145/2882903.2882952>
- [39] Zhuohang Lai, Qiong Luo, and Xiaoying Jia. 2018. Revisiting Multi-Pass Scatter and Gather on GPUs. In *Proceedings of the 47th International Conference on Parallel Processing (Eugene, OR, USA) (ICPP '18)*. Association for Computing Machinery, New York, NY, USA, Article 25, 11 pages. <https://doi.org/10.1145/3225058.3225095>
- [40] Zhuohang Lai, Xibo Sun, Qiong Luo, and Xiaolong Xie. 2021. Accelerating Multi-Way Joins on the GPU. *The VLDB Journal* 31, 3 (nov 2021), 529–553. <https://doi.org/10.1007/s00778-021-00708-y>
- [41] Rubao Lee, Minghong Zhou, Chi Li, Shenggang Hu, Jianping Teng, Dongyang Li, and Xiaodong Zhang. 2021. The Art of Balance: A RateupDB™ Experience of Building a CPU/GPU Hybrid Database Product. *Proc. VLDB Endow.* 14, 12 (jul 2021), 2999–3013. <https://doi.org/10.14778/3476311.3476378>
- [42] Jing Li, Hung-Wei Tseng, Chunbin Lin, Yannis Papakonstantinou, and Steven Swanson. 2016. HippogriffDB: Balancing I/O and GPU Bandwidth in Big Data Analytics. *Proc. VLDB Endow.* 9, 14 (oct 2016), 1647–1658. <https://doi.org/10.14778/3007328.3007331>

- [43] Clemens Lutz, Sebastian Breß, Steffen Zeuch, Tilmann Rabl, and Volker Markl. 2020. Pump Up the Volume: Processing Large Data on GPUs with Fast Interconnects. In *Proceedings of the 2020 ACM SIGMOD International Conference on Management of Data* (Portland, OR, USA) (SIGMOD '20). Association for Computing Machinery, New York, NY, USA, 1633–1649. <https://doi.org/10.1145/3318464.3389705>
- [44] Clemens Lutz, Sebastian Breß, Steffen Zeuch, Tilmann Rabl, and Volker Markl. 2022. Triton Join: Efficiently Scaling to a Large Join State on GPUs with Fast Interconnects. In *Proceedings of the 2022 International Conference on Management of Data* (Philadelphia, PA, USA) (SIGMOD '22). Association for Computing Machinery, New York, NY, USA, 1017–1032. <https://doi.org/10.1145/3514221.3517911>
- [45] S. Manegold, P. Boncz, and M. Kersten. 2002. Optimizing main-memory join on modern hardware. *IEEE Transactions on Knowledge and Data Engineering* 14, 4 (July 2002), 709–730. <https://doi.org/10.1109/TKDE.2002.1019210>
- [46] Stefan Manegold, Peter Boncz, Niels Nes, and Martin Kersten. 2004. Cache-Conscious Radix-Declasser Projections. In *Proceedings of the Thirtieth International Conference on Very Large Data Bases - Volume 30* (Toronto, Canada) (VLDB '04). VLDB Endowment, 684–695.
- [47] Supun Nakandala, Karla Saur, Gyeong-In Yu, Konstantinos Karanasos, Carlo Curino, Markus Weimer, and Matteo Interlandi. 2020. A Tensor Compiler for Unified Machine Learning Prediction Serving. In *14th USENIX Symposium on Operating Systems Design and Implementation (OSDI 20)*. USENIX Association, 899–917. <https://www.usenix.org/conference/osdi20/presentation/nakandala>
- [48] Adam Paszke, Sam Gross, Francisco Massa, Adam Lerer, James Bradbury, Gregory Chanan, Trevor Killeen, Zeming Lin, Natalia Gimelshein, Luca Antiga, Alban Desmaison, Andreas Kopf, Edward Yang, Zachary DeVito, Martin Raison, Alykhan Tejani, Sasank Chilamkurthy, Benoit Steiner, Lu Fang, Junjie Bai, and Soumith Chintala. 2019. PyTorch: An Imperative Style, High-Performance Deep Learning Library. In *Advances in Neural Information Processing Systems 32*, H. Wallach, H. Laroche, A. Beygelzimer, F. d'Alché Buc, E. Fox, and R. Garnett (Eds.). Curran Associates, Inc., 8024–8035. <http://papers.neurips.cc/paper/9015-pytorch-an-imperative-style-high-performance-deep-learning-library.pdf>
- [49] Johns Paul, Bingsheng He, Shengliang Lu, and Chiew Tong Lau. 2020. Revisiting hash join on graphics processors: A decade later. *Distributed and Parallel Databases* 38 (2020), 771–793.
- [50] Johns Paul, Jiong He, and Bingsheng He. 2016. GPL: A GPU-Based Pipelined Query Processing Engine. In *Proceedings of the 2016 International Conference on Management of Data* (San Francisco, California, USA) (SIGMOD '16). Association for Computing Machinery, New York, NY, USA, 1935–1950. <https://doi.org/10.1145/2882903.2915224>
- [51] Johns Paul, Shengliang Lu, Bingsheng He, and Chiew Tong Lau. 2021. MG-Join: A Scalable Join for Massively Parallel Multi-GPU Architectures. In *Proceedings of the 2021 International Conference on Management of Data* (Virtual Event, China) (SIGMOD '21). Association for Computing Machinery, New York, NY, USA, 1413–1425. <https://doi.org/10.1145/3448016.3457254>
- [52] Mark Raasveldt and Hannes Mühleisen. 2019. DuckDB: An Embeddable Analytical Database. In *Proceedings of the 2019 International Conference on Management of Data* (Amsterdam, Netherlands) (SIGMOD '19). Association for Computing Machinery, New York, NY, USA, 1981–1984. <https://doi.org/10.1145/3299869.3320212>
- [53] Viktor Rosenfeld, Sebastian Breß, and Volker Markl. 2022. Query Processing on Heterogeneous CPU/GPU Systems. *ACM Comput. Surv.* 55, 1, Article 11 (jan 2022), 38 pages. <https://doi.org/10.1145/3485126>
- [54] Ran Rui, Hao Li, and Yi-Cheng Tu. 2020. Efficient Join Algorithms for Large Database Tables in a Multi-GPU Environment. *Proc. VLDB Endow.* 14, 4 (dec 2020), 708–720. <https://doi.org/10.14778/3436905.3436927>
- [55] Ran Rui and Yi-Cheng Tu. 2017. Fast Equi-Join Algorithms on GPUs: Design and Implementation. In *Proceedings of the 29th International Conference on Scientific and Statistical Database Management* (Chicago, IL, USA) (SSDBM '17). Association for Computing Machinery, New York, NY, USA, Article 17, 12 pages. <https://doi.org/10.1145/3085504.3085521>
- [56] Amazon Web Service. [n.d.]. AWS EC2 Instance Types. online. <https://aws.amazon.com/ec2/instance-types/>
- [57] Anil Shanbhag, Samuel Madden, and Xiangyao Yu. 2020. A Study of the Fundamental Performance Characteristics of GPUs and CPUs for Database Analytics. In *Proceedings of the 2020 ACM SIGMOD International Conference on Management of Data* (Portland, OR, USA) (SIGMOD '20). Association for Computing Machinery, New York, NY, USA, 1617–1632. <https://doi.org/10.1145/3318464.3380595>
- [58] Ambuj Shatdal, Chander Kant, and Jeffrey F. Naughton. 1994. Cache Conscious Algorithms for Relational Query Processing. In *Proceedings of the 20th International Conference on Very Large Data Bases (VLDB 94)*. Morgan Kaufmann Publishers Inc., San Francisco, CA, USA, 510–521.
- [59] Lakshmi Kant Shrinivas, Sreenath Bodagala, Ramakrishna Varadarajan, Ariel Cary, Vivek Bharathan, and Chuck Bear. 2013. Materialization strategies in the Vertica analytic database: Lessons learned. In *2013 IEEE 29th International Conference on Data Engineering (ICDE)*, 1196–1207. <https://doi.org/10.1109/ICDE.2013.6544909>
- [60] Panagiotis Sioulas, Periklis Chrysogelos, Manos Karpapothakis, Raja Apuswamy, and Anastasia Ailamaki. 2019. Hardware-Conscious Hash-Joins on GPUs. In *2019 IEEE 35th International Conference on Data Engineering (ICDE)*, 698–709. <https://doi.org/10.1109/ICDE.2019.00068>
- [61] Wenbo Sun, Asterios Katsifodimos, and Rihan Hai. 2023. An Empirical Performance Comparison between Matrix Multiplication Join and Hash Join on GPUs. In *2023 IEEE 39th International Conference on Data Engineering Workshops (ICDEW)*, 184–190. <https://doi.org/10.1109/ICDEW58674.2023.00034>
- [62] Neil C. Thompson and Svenja Spanuth. 2021. The Decline of Computers as a General Purpose Technology. *Commun. ACM* 64, 3 (feb 2021), 64–72. <https://doi.org/10.1145/3430936>
- [63] TPC. 2023. TPC-DS Benchmark. <http://www.tpc.org/tpcds/>. Accessed: November 13, 2023.
- [64] TPC. 2023. TPC-H Benchmark. <http://www.tpc.org/tpch/>. Accessed: November 13, 2023.
- [65] Makoto Yabuta, Anh Nguyen, Shinpei Kato, Masato Edahiro, and Hideyuki Kawashima. 2017. Relational Joins on GPUs: A Closer Look. *IEEE Transactions on Parallel and Distributed Systems* 28, 9 (2017), 2663–2673. <https://doi.org/10.1109/TPDS.2017.2677451>
- [66] Bobbi W. Yogatama, Weiwei Gong, and Xiangyao Yu. 2022. Orchestrating Data Placement and Query Execution in Heterogeneous CPU-GPU DBMS. *Proc. VLDB Endow.* 15, 11 (jul 2022), 2491–2503. <https://doi.org/10.14778/3551793.3551809>
- [67] Yuan Yuan, Rubao Lee, and Xiaodong Zhang. 2013. The Yin and Yang of Processing Data Warehousing Queries on GPU Devices. *Proc. VLDB Endow.* 6, 10 (aug 2013), 817–828. <https://doi.org/10.14778/2536206.2536210>
- [68] Mark Zhao, Niket Agarwal, Aarti Basant, Buğra Gedik, Satadru Pan, Mustafa Ozdal, Rakesh Komuravelli, Jerry Pan, Tianshu Bao, Haowei Lu, Sundaram Narayanan, Jack Langman, Kevin Wilfong, Harsha Rastogi, Carole-Jean Wu, Christos Kozyrakis, and Parik Pol. 2022. Understanding Data Storage and Ingestion for Large-Scale Deep Recommendation Model Training: Industrial Product. In *Proceedings of the 49th Annual International Symposium on Computer Architecture* (New York, New York) (ISCA '22). Association for Computing Machinery, New York, NY, USA, 1042–1057. <https://doi.org/10.1145/3470496.3533044>